Journal of Civil Structural Health Monitoring (2021) 11:1093–1112
https://doi.org/10.1007/s13349-021-00495-8

APPLICATION BASED

Experimental verification for load rating of steel truss bridge using an improved Hamiltonian Monte Carlo-based Bayesian model updating

Shubham Baisthakur[1] · **Arunasis Chakraborty**[2]

Received: 30 November 2020 / Revised: 16 March 2021 / Accepted: 22 May 2021 / Published online: 19 June 2021

Abstract

The load rating of a steel truss bridge is experimentally identified in this study using an improved Bayesian model updating algorithm. The initial element model is sequentially updated to match the static and dynamic characteristics of the bridge. For this purpose, a modified version of the Hamiltonian Monte Carlo (HMC) simulation is adopted for closed-form candidate generation that helps in faster convergence compared to the Markov Chain Monte Carlo simulation. The updated model works as a digital twin of the original structure to predict its load-carrying capacity and performance under proof or design load. The proposed approach incorporates in-situ conditions in its formulation and helps to reduce the risk involved in bridge load testing at its full capacity. The rating factor for each member is estimated from the updated model, which also indicates the weak links and possible failure mechanism. The efficiency of the improved HMC-based algorithm is demonstrated using limited sensor data, which can be easily adopted for other existing bridges.

Keywords Bayesian Inference · Markov Chain Monte Carlo Simulation · Hamiltonian Monte Carlo Simulation · Finite element model updating · Bridge rating

1 Introduction

Condition assessment and bridge load rating have remained an active area of research in the last few decades as new methodologies (both analytical and experimental) are developed to meet the ever-increasing complexities. In this context, rating factor analysis establishes the safe load-carrying capacity of a bridge. It is evaluated for every structural member due to the force generated for a given live load. Ultimately the minimum rating factor among the members governs the load-carrying capacity of a bridge, which in turn dictates its load limit (i.e. posting), repairing, or closure. Thus, rating analysis is essential to ensure the safety and well functioning of any bridge. It is particularly important for bridges, which are close to their design life. Also, it is necessary for the bridges, which are expected to carry loads higher than their design class.

Visual inspection of a bridge is the first step to assessing its health and assigning a qualitative rating factor based on specific guidelines [1]. It can only provide a limited understanding of bridge health based on some preliminary analysis or any noticeable physical deterioration. However, it is not sufficient for capacity estimation and often provides subjective assessment based on the judgement of the inspector. Phares et al. [2] highlighted this aspect of visual inspection for condition assessment of a bridge. Visual inspection supplemented by detailed testing provides more evidence to ascertain the health and load-carrying capacity of any bridge. Thus, designers and engineers have actively pursued vibration-based rating analysis in the recent past [3–8]. In this context, field tests are performed on a bridge to study its response under controlled loading. Bridge load tests are classified as Proof Load Test (PLT) and Diagnostic Test (DT) based on the magnitude of load used for testing. A factored design load is used in the proof load test to investigate bridge behaviour. The test load is gradually increased to its design value (i.e. factor is one) unless any distress is

✉ Arunasis Chakraborty
arunasis@iitg.ac.in

Shubham Baisthakur
baisthakurss@gmail.com

[1] Larson & Toubro ECC, Chennai 600089, India

[2] Civil Engineering Department, Indian Institute of Technology Guwahati, Assam, India

observed. Generally, this test is performed before opening a newly constructed bridge to ascertain its capacity or for an existing bridge to establish the available strength in the light of ageing and subsequent deterioration. Thus, proof load test serves as a benchmark to identify the actual load-carrying capacity [5, 9, 10]. Since the test load is gradually increased, proof load test faces a potential risk of permanently damaging a bridge. Thus, it also involves significant cost to ensure the safety of the structure and its surrounding during the experiment [11]. However, attempts have been made to make this test more feasible as it gives an accurate estimation of the capacity [4, 12, 13]. Faber et al. [12] developed a reliability-based formulation to calibrate the intensity of proof load to ensure target reliability considering deterioration, failure modes, and uncertainty in bridge resistance. Contrary to the proof load test, diagnostic test limits the magnitude of live load to a level that is known to be safe for a bridge. The recorded responses (e.g. acceleration, strain, displacement, tilt) in this test are further analyzed to assess the bridge health. This test aims to document the structural response under various loading and ambient conditions, which can be used for model calibration. It is frequently conducted for rating analysis [14] due to its cost-effectiveness and minimal impact on the bridge operations. Previous studies [15–17] firmly established the potential of diagnostic tests for the health monitoring and subsequent rating analysis of a bridge.

Since a lower load than the designed capacity of any bridge is used in the Diagnostic Test, it largely depends on the calibrated model to assess the ultimate capacity. In this context, model calibration for condition assessment and load rating offers several challenges, where inconsistencies between the actual and the model predicted behaviour is well known in the literature [18, 19]. Common causes behind this difference are material deterioration[12], bearing restraint [19], unintended composite action [20, 21], load distribution effects [22] and secondary effects [18]. Thus, a finite element model serves as an approximate representation of an actual bridge due to different assumptions and uncertainties involved in modelling. These models need to be calibrated using measurements so that they can replicate the actual behaviour. In this process, specific model parameters are selected based on the physical condition, which are tuned so that the model predicted behaviour is consistent with the actual response [3, 23]. These parameters are adjusted until the required level of consistency is achieved. Catbas et al. [24] and Dong et al. [25] used this approach to obtain a more practical distribution factor for the existing bridges. They highlighted the conservative nature of these factors given in the guidelines [26]. Since the calibrated model can closely replicate the actual behaviour, rating factor analysis performed on such models are expected to offer identical results obtained from the bridge load test [21, 27–29]. In this context, deterministic optimization is commonly adopted for model calibration before load rating. Although the model is calibrated to match the observation, it fails to incorporate the measurement error. Also, modelling error plays a vital role in its calibration. Thus, the model calibrated using deterministic optimization is not very accurate when exposed to different loading conditions. Also, the deterministic model calibration gives a single best output of the design parameters and rules out the possibility of multiple solutions. Thus, it is often calibrated in the stochastic framework using Bayesian inference to overcome these limitations [30, 31]. This method includes measurement noise and modelling assumptions in the updating process to obtain the best possible solution. The acceptance or rejection of candidates in this method depends on the error, conditioned by the measurement noise and the modelling class.

The stochastic model updating does not offer a single best output; instead, it forms a probability distribution over the possible values of the uncertain parameter. This posterior distribution specifies the relative plausibility of each uncertain model parameter achieving a particular value. The high probability region of the posterior distribution is often concentrated in a narrow band of the parameter space. The updating algorithms use an adaptive approach to converge to the final solution [32, 33], avoiding a higher-rejection rate and the non-ergodicity in the Markov chain caused by the high probability zone. In this context, random-walk-based candidate generation schemes are popular among the researchers, where the Metropolis–Hastings algorithm or its modified versions are used to formulate the posterior distribution [32, 33]. This approach requires a large number of iteration and is computationally exhaustive when updating a complex structure. Cheung and Beck [34] developed an efficient algorithm based on Hamiltonian dynamics to expedite the convergence. In this formulation, the parameter space is mapped with a Hamiltonian system such that the solution of the governing equation generates the required candidate states. Conventionally, the leapfrog algorithm [34, 35] is used to solve the governing equations. This technique requires numerical integration of the objective function with respect to the uncertain parameters. Due to this reason, the computational cost increases directly with the rise in unknown parameter and complexity of the model. In this context, a closed-form candidate generation scheme was developed in the literature [36, 37], which performed better than the leapfrog algorithm.

Besides the Bayesian approach, recent advancement in bridge rating has witnessed Artificial Neural Network [38], Machine learning [39], Multi-regression-based framework [40], Big data analytic [41] and Weigh-In-Motion studies [42]. Some of these studies use global system-based reliability analysis to assess the health and safety [43–45]. A complete review of different bridge rating methodologies with the benefit of load testing based on a cost–benefit analysis is presented by Alampalli et al. [46]. These authors also present the scientific background for bridge load testing [47], which contains new proposals for interpreting the results of diagnostic load tests, loading protocols, and load ratings based on the results of proof load tests.

2 Problem formulation

The literature review presented above highlights the current status of the bridge rating. It also discusses various load-testing approaches and the importance of model calibration for rating analysis and capacity estimation. In this context, measurement and modelling uncertainties play a vital role in the quality of results. Although different deterministic and stochastic algorithms are available in the literature, there is further scope for their improvements. Besides theoretical developments, filed implementation of these models for actual bridge rating has equal, if not greater, importance. With this in view, the present study aims to investigate the performance of an efficient HMC-based stochastic model calibration, which can address the difficulties faced by existing bridge rating practices. This approach uses a calibrated model to predict the load-carrying capacity, which is validated experimentally. Thus, the following objectives are set for this work

1. Develop a modified Hamiltonian Monte Carlo algorithm for stochastic model updating using an efficient closed-form candidate generation technique and perform a comparative analysis with the conventional Markov Chain Monte Carlo approach.
2. Experimentally validate the proposed model updating strategy using diagnostic test of a steel truss bridge. Use the calibrated model to predict the rating factor under different loading scenario.
3. The steel truss bridge used in this study has experienced misalignment at some of its joints during fabrication. Thus, the present work also aims to investigate the impact of the joint misalignment on the dynamics of steel truss bridge and its ultimate load-carrying capacity.

3 Overview of bridge rating

The bridge load rating is a process of quantifying its load-carrying capacity in its as-built or in-situ condition. The design of a bridge considers all possible loads (e.g. live load, earthquake load, wind load) and their combinations. Among them, the capacity of a bridge in terms of the live load is most important. Thus, the rating of a bridge is formulated by the following equation

$$\gamma_D D + \gamma_L (L + I) < C \tag{1}$$

In the above equation, C is capacity, D is dead load effect and $(L + I)$ represents the combined effect of live load and impact. The factors γ_D and γ_L in Eq. (1) correspond to dead and live load, respectively. Rearranging this equation leads to the rating factor in the following compact form

$$\mathrm{RF} = \frac{C - \gamma_D D}{\gamma_L (L + I)} \tag{2}$$

This non-dimensional number is expressed as the reserve strength ratio after removing the effect of the permanent load to the live load effect. It is a unique number corresponding to a pre-selected class of live load. The rating factor is evaluated at the component level, and the minimum rating factor governs the load-carrying capacity of a bridge. Here, it may be noted that a rating factor less than one does not necessarily imply the collapse of a structure due to the high level of indeterminacy that is usually present in the design. However, this factor indicates the under-performance of a particular member, highlighting the possibility of failure due to a chain of events that might originate from this element.

The bridge rating can be carried out at two levels: inventory level rating and operating level rating, depending upon the type of load used for testing. The inventory level rating uses a nominal live load that can traverse over the bridge indefinitely. In contrast, the operating level rating considers the maximum live load that a bridge might be exposed to during its entire lifetime. The factors γ_D and γ_L are chosen depending upon the type of rating. So, the rating formulation in Eq. (2) can be modified to suit the codal guidelines and the traffic characteristics of a particular region. In the context of Indian standard specifications and traffic characteristics, the expression for rating factor can be formulated as

$$\mathrm{RF} = \frac{C - \gamma_D D}{\gamma_L (\mathrm{OF}) L (1 + \mathrm{IF})} \tag{3}$$

In this equation, OF and IF are the overload factor and impact factor, respectively. The detailed description of Overload Factor (OF) is specified in IRC:SP:37-2010 [48], which is the guideline released by the Indian Road Congress (IRC) to establish a standard procedure to access the strength, evaluate the safe load carrying capacity and provide information regarding the rating of a bridge. This guideline also presents a systematic approach for structural assessment and practical features of traffic characteristic in India. The OF is recommended in this guideline to address the general tendency of the transport operators to increase freight beyond the limits specified by the legal bodies. This factor is based on the actual survey of the gross weight of vehicles traversing over a bridge, but in any case, it should not be less than the average overload factor mentioned in the same guideline. On the other hand, the Impact Factor (IF) is a provision made to express the dynamic effect of moving vehicles on the bridge. This factor depends on the live load characteristics, span, and type of the bridge. The OF for standard load classes and bridge span are mentioned in IRC:6-2016 [49], which outlines the design and construction of road bridges in India.

The expression for load rating in Eq. (3) offers a compact framework for quantifying the load-carrying capacity of any bridge. It involves a detailed structural analysis for the dead load effect while the live load effects are observed from the actual testing. In this context, engineers often face difficulties with existing bridges that have undergone deterioration over time. The in-situ condition needs to be assessed before dead load analysis and testing using an appropriate live load. Thus, condition assessment is a key step for any meaningful rating analysis. Different options for condition assessment exist in the literature [27, 38, 40, 41]. Among them, Bayesian inference is a popular tool, which is adopted in this study.

4 Hybrid Monte Carlo simulation-based Bayesian model updating

The inconsistency between a model-predicted response and the actual behaviour obtained from testing has been widely reported in the literature [2, 18, 23]. In this context, the uncertainties in modelling can be categorized as parametric uncertainty and modelling uncertainty. The first category indicates the uncertainty caused by a particular value of a parameter in modelling whose exact value may vary. It is commonly encountered due to inherent variability of some parameters due to workmanship, quality control or ageing, e.g. the compressive strength of concrete whose exact spatial variation in a structure is difficult to predict. The modelling uncertainty is generally caused due to the simplification involved in modelling structural components and boundary conditions. In bridges, modelling uncertainty is mainly attributed to bearings and other joints. For example, the bearings, which are modelled as simply supported boundary conditions, often offer restraint, leading to a significant reduction of span moments. These differences should be logically eliminated from a finite element model that acts as a digital twin of the actual structure.

The stochastic model updating in the Bayesian framework uses an optimization technique, which is formulated so that the observations and the modelling assumptions are given due importance while arriving at the final updated model. In this approach, the uncertain parameters θ are first identified, which are then updated by conditioning them using measurements $\mathbf{D}$ and the mathematical model class $\mathbf{C}$. The model updating in this approach is presented by the following form

$$p(\theta|\mathbf{D},\mathbf{C}) = \mathbf{K}_0 p(\mathbf{D}|\theta,\mathbf{C})p(\theta|\mathbf{C}) \tag{4}$$

where $p(\theta|\mathbf{D},\mathbf{C})$, i.e. posterior pdf, describes the probability of uncertain parameter θ given the actual structural response $\mathbf{D}$ and the model class $\mathbf{C}$. The term $p(\mathbf{D}|\theta,\mathbf{C})$ is the likelihood function, which quantifies the error, i.e. difference between the measurement and the model predicted response. Thus, the likelihood of obtaining the structural response $\mathbf{D}$ for a specified set of model parameter values θ can be quantified. The term $p(\theta|\mathbf{C})$, i.e. prior pdf, represents the initial perception of the uncertain parameter θ_i. This updating formulation modifies the initial understanding of the uncertain parameters [i.e. $p(\theta|\mathbf{C})$] by incorporating observations [i.e. $p(\mathbf{D}|\theta,\mathbf{C})$] and proposes a more accurate understanding of the parameters [i.e. $p(\theta|\mathbf{D},\mathbf{C})$]. In this process, a number of samples are generated using a suitable simulation technique, and the posterior probability for each set of θ is evaluated using Eq. (4). Blending these three terms offers a holistic model updating framework while precisely replicating the field condition.

The stochastic model updating in the Bayesian framework involves Markov Chain Monte Carlo (MCMC) simulation [32, 33] to generate a candidate state. The random walk nature of this candidate generation technique using the Metropolis–Hastings algorithm or its advanced versions leads to frequent diversion from the probable solution and subsequently slowing down the convergence. Due to this reason, these algorithms require a large number of iterations to arrive at the final updated model, and hence they are computationally exhaustive for large structures like bridges. This paper presents an alternative approach to expedite the simulation process using principles of Hamiltonian dynamics. In this method, the candidates are simulated by mimicking the time evolution of a Hamiltonian system. The governing equation is generally solved using the leapfrog algorithm [36], a popular mathematical tool to explore the region of high probability within the parameter space using the gradient of the posterior pdf. In this process, the gradient is used to generate the next candidate based on the current state of the system, which is also a time-consuming process. The computational effort increases exponentially with the increase of dimension, i.e. number of unknown parameters. Thus, an efficient closed-form candidate generation scheme is adopted in this work, which is explained below.

An overview of the Hamiltonian dynamics for efficient candidate generation is presented here, along with the proposed sample generation scheme to bypass the leapfrog algorithm. Readers may refer to Baisthakur and Chakraborty [37] for further details on this topic. The parameter vector θ is considered analogous to the position vector, say β, of a Hamiltonian system. Further, an auxiliary variable, say γ, is generated to complete the position–momentum-phase space. The potential energy (V) and kinetic energy (K) are defined in terms of position and momentum as

$$V(\beta) = -\log(p(\beta|D, C)) \tag{5a}$$

$$K(\gamma) = \frac{\gamma^T M^{-1}\gamma}{2} \tag{5b}$$

The Hamiltonian for this system is defined as

$$\begin{aligned} H(\beta,\gamma) &= V(\beta) + K(\gamma) \\ &= -\,log(p(\beta|D, C)) + \frac{\gamma^T M^{-1}\gamma}{2} \end{aligned} \tag{6}$$

The canonical ensemble for this system is defined by the summation of potential energy (V) and kinetic energy (K), i.e.

$$f(x) = \frac{1}{Z}e^{-H(\beta,\gamma)} = \frac{1}{Z}p(\beta|D, C)e^{\frac{\gamma^T M^{-1}\gamma}{2}} \tag{7}$$

where Z is a normalizing constant such that the area under the pdf is equal to unity. From this equation, it is clear that the time evolution of this system can generate the position–momentum-phase space such that the position parameter follows the target probability distribution, while the auxiliary momentum variable follows the Gaussian distribution with zero mean and covariance matrix M. The governing Hamiltonian equations for this system are given by

$$\frac{d\beta}{dt} = \frac{\partial H}{\partial \gamma} \tag{8a}$$

$$\frac{d\gamma}{dt} = -\frac{\partial H}{\partial \beta} \tag{8b}$$

These equations can be solved numerically by assuming an initial guess [$\beta(0)$,$\gamma(0)$]. The position and momentum of the particle after some finite time δt are obtained as

$$\beta(t+\delta t) = \beta(t) + \delta t M^{-1}\{\gamma(t) - \frac{\delta t}{2}\Delta V[\beta(t)]\} \tag{9a}$$

$$\gamma(t+\delta t) = \gamma(t) - \frac{\delta t}{2}\{\Delta V[(\beta(t)] + \Delta V[(\beta(t+\delta t)]\} \tag{9b}$$

This scheme requires numerical evaluation of the gradient ΔV. For a particular case, where the target pdf follows Standard Gaussian distribution and M becomes an identity matrix, the Hamiltonian takes the following form

$$H(\beta,\gamma) = \frac{\beta^T\beta}{2} + \frac{\gamma^T\gamma}{2} \tag{10}$$

The analytical solution of the time evolution for the above system can be expressed as

$$\beta(t) = \gamma_{\text{in}}\sin t + \beta_{\text{in}}\cos t \tag{11a}$$

$$\gamma(t) = \gamma_{\text{in}}\cos t - \beta_{\text{in}}\sin t \tag{11b}$$

where β_{in} and γ_{in} are the initial position and momentum, respectively. The time parameter t for candidate generation using the above formulation is arbitrarily assigned such that $t \in [-\pi/2, \pi/2]$.

In general, the high-probability region of the target posterior density function is concentrated within a narrow band of the parameter space. The posterior pdf within this narrow margin leads to frequent rejection of the candidate states. Thus, the Markov chain in the Metropolis–Hastings algorithm or its modified version is often trapped leading to a non-ergodic state. Various researchers have addressed this issue using a sequence of intermediate pdfs [32, 33] that gradually converge to the target pdf, which is given by

$$p_i = c_i\exp\left[-\frac{J_g(\theta)}{2\epsilon_i^2}\right] \tag{12}$$

This study uses an adaptive scheme proposed by Baisthakur and Chakraborty [37] for generating the intermediate pdfs, where the parameter ϵ^2 is evaluated as follows

$$\epsilon_i^2 = \frac{-J_g(\mu_i)}{2\ln r} \times \frac{k}{i} \tag{13a}$$

$$r = \frac{p(\theta|D, C)}{p(\theta|C)} \tag{13b}$$

In Eq. (13a), the term $J_g(\mu_i)$ is the goodness-of-fit function quantifying the error between the measurement and the model response for a set of uncertain parameters evaluated at their respective mean values. The terms r and k are tuned to achieve the desired rate of acceptance for the candidate states.

Any updating scheme, in general, uses maximum computational cost for solving the finite element model. Thus, the primary approach for developing a computationally efficient model updating algorithm is to reduce the number of model evaluations. The candidate generation using the leapfrog algorithm requires numerical evaluation of gradient of the potential energy (V) (i.e. as in Eqs. 9a and b). Since the potential energy function is the logarithm of the target pdf, their gradient evaluation involves the complete finite element model. Moreover, the number of gradient evaluations is directly proportional to the dimension of the parameter space. Additionally, the Leapfrog algorithm being a time-stepping algorithm, uses a finite number of time steps L to generate a new state $\theta(t+\delta t)$ based on the current state $\theta(t)$. Therefore, the number of finite element model evaluation in this approach to generate a candidate state is $n_c = 2NL$, where N is the dimension of the parameter space. Due to this reason, the computational cost for model updating increases directly with the increase of dimension of $\theta(t)$. Hence, it becomes increasingly prohibitive for higher-order parameter space and complex finite element models.

The proposed HMC algorithm uses a closed-form solution presented in Eq. (11) for generating the candidate states. The computational time required for candidate generation is independent of the complexity of the finite element model and the dimension of the parameter space since this scheme does not require the evaluation of a finite element model for candidate generation. Therefore, it is computationally more efficient for finite element model updating of large structures. In this context, candidate generation in conventional MCMC also does not require finite element model evaluation. However, it requires a large number of candidates for convergence due to the random-walk nature of candidate generation that has lower acceptance rate. The Hamiltonian approach using closed-form candidate generation is more efficient than the random walk-based MCMC method in exploring the high-probability region of target pdf. This feature of the proposed algorithm will be demonstrated further in the numerical analysis.

5 The Pasakha steel bridge

In this study, a steel truss bridge is used to demonstrate the efficiency of the modified Hamiltonian Monte Carlo simulation-based finite element model updating for bridge rating. This bridge (also known as Pasakha bridge) is located on Pasakha-Monitor road in Bhutan, where it crosses over the Singi-Chu river in mountainous terrain. The bridge has a span of 55 m and width of 12 m. The super-structure is made of steel truss on bearings at both ends on top of 2 m high abutments made of M35 grade concrete. The bridge deck is 185 mm thick and is made of the same grade of concrete. The deck slab is supported by 23 steel floor beams, spaced at 2.5 m intervals over the entire span. The dimensions of the bridge super-structure (i.e. Fig. 1a) are provided in the Appendix. It is designed following the Indian standard specifications [49–52] to carry the IRC-70R class live load. This live load corresponds to a tracked vehicle with a gross weight of 700 kN or a wheeled vehicle with a gross weight of 1000 kN. The tracked vehicle has a contact length of 4.57 m, and the nose to tail length of the vehicle is 7.92 m. The wheeled vehicle has a total of seven axles with a total length of 15.22 m. The schematic diagram of the wheeled loading pattern in this class is presented later in this article.

The bridge was fabricated on-site using form-work in the recent past. During its fabrication, a sudden flash flood in the river led to the distortion of the scaffolding, which ultimately reflected in the misalignment of some joints as shown in Fig. 1b. A detailed survey was carried out to identify the positions, and the maximum dislocation of the top joints was found to be 0.49% of the span. The survey also revealed that the bottom joints were least affected by the flash flood due to the rigidity provided by the deck slab. During the initial test after its construction with a load far below its designated class, the bridge experienced severe vibration. Due to this reason, an experimental load rating was planned to assess the impact of joint misalignment on the performance of this bridge and to determine its safe load-carrying capacity.

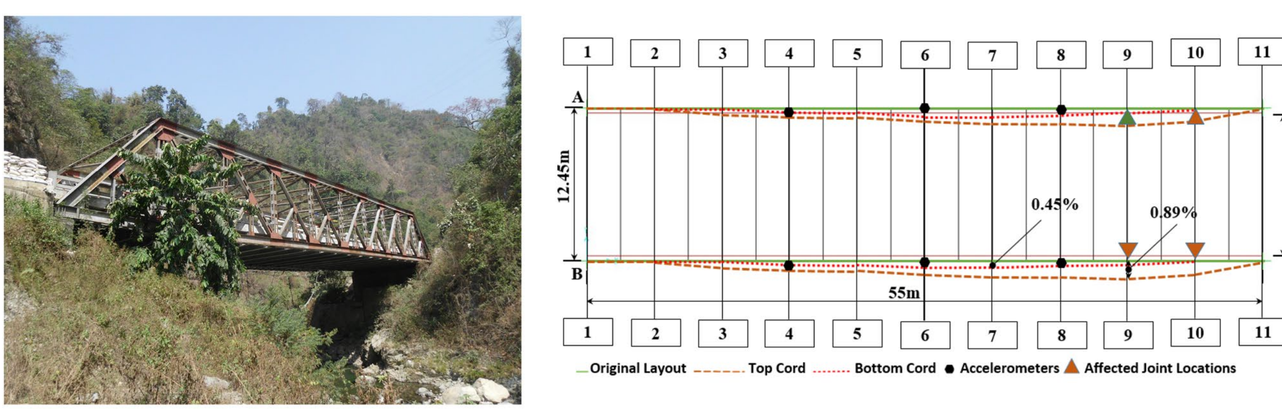

(a) (b)

Fig. 1 Details of bridge; **a** Pasakha Bridge and **b** survey data for joint misalignment

6 Bridge testing and data acquisition

As stated above, the Pasakha bridge is considered for experimental verification in this study to determine the effects of joint misalignment on its load rating. This, in turn, demands in-situ condition assessment followed by rating factor estimation. Thus, a static load test is conducted first to investigate the load vs. deflection behaviour of the bridge. It is followed by a diagnostic load test for condition assessment and Bayesian model updating using the proposed HMC algorithm for capacity estimation.

6.1 Static load test

The static load test is adopted to study the overall performance of the bridges. The Indian Road Congress guideline [48] recommends this test for rating analysis of a newly constructed or an operating/existing bridge. The load can be applied using a vehicle or by assembling static loads in the form of a wheel or track imprints to match the loading pattern of a particular class of vehicle. For this test, the loading pattern is created to resemble a class 70R tracked vehicle occupying the middle of the deck, which has a total load of 128 MT. The additional weight over the gross tonnage of 70R class for a tracked vehicle (i.e. 100 MT) is to account for the dynamic amplification. The spacings of loading imprints as per the codal provisions are maintained, and the equal distribution of load is ensured by placing the rolled steel sections across the imprints. The platform supported on the steel sections is loaded using the preweighed sandbags. The incremental loading of the platform is done to avoid any untoward distress in the bridge. It is particularly recommended where the load-carrying capacity of the bridge is to be identified. In addition to the load placed at the mid-span (BRLL), a permanent pavement live load (FPLL) of 2.23 kN/m^2 is also placed throughout the footpath as considered in the design.

The load is increased incrementally at 30, 50, 70, 90, and 100% of its absolute magnitude. The incremental load is added when the deformations due to the previous load are stabilized, and the necessary observations (such as the deflection at critical sections, appearance of cracks, and bearing deflections) are recorded. During this process, settlement of the bearings are also recorded to eliminate their effects on the mid-span deflection. The deflection of the abutments on either side is measured using a dial gauge during each load increment. The average observed bearing settlement (δ_b) is subtracted from the measured mid-span deflection (δ_{ms}). Further, the ambient temperature during testing (T) is recorded at regular intervals to address the deflections caused due to thermal deformations. The temperature correction is then applied to the bearing settlement, and the value of the mid-span deflection is obtained as the final deflection caused due to loading alone (δ_f). For temperature correction, the thermal response is studied in consecutive days at a one-hour interval over the period for which the load test is performed. This deflection value is checked against the permissible deflection (δ_p) prescribed by the IRC guidelines [53] to compare the actual behaviour of the structure against its expected behaviour. The

Table 1 Static load test data

Sr no.	Loading stage	Time (BST)	δ_{ms}	δ_b	δ_p	δ_f	Gross load	T (°C)
Loading								
1	Before start of loading	1000	–	–	–	–	–	21
2	FPLL@227 kG per Sqm	1135	1.78	0.025	3.1	1.755	18.727	23
3	FPLL + 30% BRLL	1305	5.40	0.030	9.8	5.370	57.127	24
4	FPLL + 50% BRLL	1545	17.29	0.175	14.3	17.115	82.727	24
5	FPLL + 70% BRLL	1755	23.46	0.265	18.8	23.195	107.000	21
6	FPLL + 70% BRLL	1800	23.46		18.8	23.460	107.000	21
7	FPLL + 70% BRLL	1830	23.84		18.8	23.840	107.000	21
8	FPLL + 70% BRLL	1920	24.15		18.8	24.150	107.000	21
9	FPLL + 70% BRLL	1940	24.25		18.8	24.250	107.000	21
Unloading (10% reduction in weight)								
1	FPLL + 60% BRLL	2035	22.61			22.610	95.527	20.5
Further unloading								
2	FPLL + 30% BRLL	1820	15.76	0.115		15.645	57.127	19
3	FPLL	1930	11.88	0.080		11.800	18.727	19
4	NIL	2110	11.51	0.045		11.465	0.000	18

FPLL refers to the footpath live Load while BRLL refers to bridge live load. Loading stopped at FPLL + 70% BRLL due to an abnormal rise in deflection deflections observed during testing and other relevant information are presented in Table 1. From this test, it can be observed that the recorded bridge deflection exceeds the allowable deflection value at 50% LL value. Subsequently, a 20% increase in LL causes an abnormal rise in the bridge deflection. Due to this excessive deformation and corresponding over-stress, the loading is stopped to avoid permanent damage. Up to this stage, the deformation kept on increasing with the live load. The unloading is carried out in a sequence of 60, 30, and 0%. After the complete removal of LL, the bridge is found to have an accumulated deformation of 9.71 mm. These observations from the static load test provide an overview of the in-situ condition, and the deformation pattern to compare them with the model predicted bridge behaviour. Although these observations are used for the initial tuning, it does not give a holistic understanding of the bridge and its performance under dynamic condition. Therefore, a diagnostic load test is carried out to establish the global dynamic behaviour under a given loading class.

6.2 Diagnostic load test for condition assessment

The diagnostic load test is conducted for better understanding the actual behaviour under controlled loading, which is known to be safe. This test is performed by passing a vehicle on the bridge at a constant speed. The finite element model of the bridge is calibrated using the recorded response to replicate its on-site characteristics. This updated model is used to evaluate the structural capacity in its as-built condition and perform other allied analysis for load rating. Thus, a 22T vehicle is selected for the diagnostic test, which passes over the bridge at a speed of 20 kmph, as shown in Fig.2a. The bridge responses are recorded using wireless accelerometers, which are analyzed to identify its modal characteristic. Three sets of wireless G-Link® LXRS® accelerometer nodes from Lord Corporation are used for this purpose. These nodes feature two integrated high-speed micro-electro-mechanical system (MEMS)-based accelerometers, producing triaxial acceleration as output. This accelerometer node offers a measurement range of ±10 g and a user-programmable sampling rate up to 4096 Hz. These sensors can be used for long-range wireless sensing up to 2 km with node-to-node synchronization of ±32 μs. The data are recorded at a sampling rate of 128 Hz and transmitted to a WSDA® base station made by the same manufacturer (refer to Fig. 2b).

Since the bridge is in remote mountainous terrain, the topography and the in-situ condition offered great difficulties to install a large number of sensors of different types. It is a practical problem for remote locations, which leaves no choice but to carry out tests with fewer instruments. Due to these limitations, the experiment is performed with a low density of instrumentation. The deterministic model calibration in this scenario may lead to misleading results and inaccurate prediction of the load-carrying capacity. Under this condition, model calibration is performed in the Bayesian framework, which addresses the uncertainty involved in test data by conditioning the probability of acceptance or rejection of model parameters. The instrumentation plan is prepared based on the preliminary modal analysis to utilize the maximum benefits of the limited sensors. Thus, the locations corresponding to maximum modal deformation are selected for the placement of accelerometer nodes. The sensors along the grid-line 6–6 shown in Fig. 1b corresponds to the maximum deformation in the first mode, while those at 4–4 and 8–8 correspond to the same in the second mode.

6.3 System identification

The acceleration responses obtained from the sensors (refer to Fig. 3a and b) are analyzed to identify the in-situ dominant modal frequencies of the Pasakha bridge using wavelet-based time–frequency analysis. For this purpose, a Morlet wavelet with a central frequency of 5 rad/s is adopted in this study. The scalogram of the vertical acceleration

(a) (b)

Fig. 2 **a** Diagnostic test of Pasakha bridge and **b** wireless accelerometer and base station

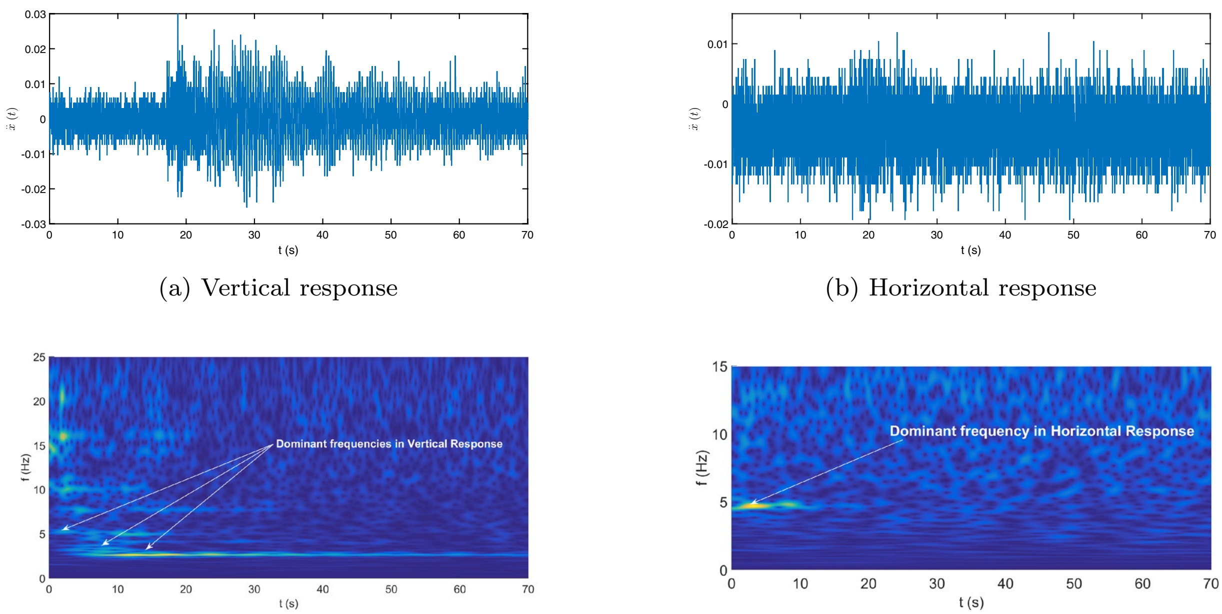

(a) Vertical response (b) Horizontal response

(c) Wavelet scalogram of vertical response (d) Wavelet scalogram of horizontal response

Fig. 3 Bridge acceleration response and wavelet based operational modal analysis

response is shown in Fig. 3c. It indicates the presence of dominant frequencies as marked in the figure, which are identified from the energy spectrum clusters as 2.733, 4.122 and 5.061 Hz. During the diagnostic test, significant rolling vibration is also reported, which does not comply with the bending behaviour. Thus, the horizontal response is also analyzed using the same signal processing technique to investigate this unwanted vibration. The scalogram of this data is presented in Fig. 3c, which indicates a mode at 4.05 Hz. The test is repeated, and each information is processed using the same time–frequency analysis to identify the dominant modal frequencies. The modal frequencies are estimated using *k*-means clustering from these energy spectra, reported in Table 2. The detailed discussion of this signal-processing technique is omitted here as it is not the theme of the present study. However, readers may refer to Mahato and Chakraborty [54] for the complete description of this operational modal analysis using wavelet-based k-means clustering.

In general, the 2D truss on either side of the bridge vibrates in the vertical plane (i.e. due to bending), where the truss members transfer loads through axial tension and compression. However, as the joints are dislocated, the member forces at a particular joint are not co-planer and generate end moments leading to significant vibration in the out-of-the-plane direction. As the joints on the right half of the bridge suffered misalignment, these joints are identified as the weak links in the model updating to match the modal frequencies obtained from the field tests as reported in Table 2. These are discussed in the following sub-section.

6.4 Finite element model updating

At first, a preliminary finite element model of the bridge is created in SAP2000®, following the as-built drawing (refer to Appendix for the details of geometric and material properties of the Pasakha bridge). In this model, the truss members are idealized as bar elements, and thin-shell elements form the bridge deck. This model is used as a reference to investigate the differences with the actual structural behaviour. It indicates the first few natural frequencies of the bridge, which, as per design, are 2.396 Hz, 4.349 Hz, and 4.940 Hz. These values are less than the frequencies observed from the operational modal analysis. These phenomena (i.e. model predicted modal frequencies are less than the identified modal frequencies) are widely encountered in bridge testing [55–57], which are generally attributed to the higher stiffness manifested at the site than the predicted values as per design. However, the static load test shows the actual deflection are more than the model predicted values, suggesting that the member stiffness offered by the as-built truss is less than its designed values. This phenomena of simultaneous higher modal frequencies and higher static deflection for Pasakha bridge are attributed to the misalignment joints. A misaligned member produces end moments at the gussets in addition to the axial force. Therefore, the joints offer partial fixity instead of

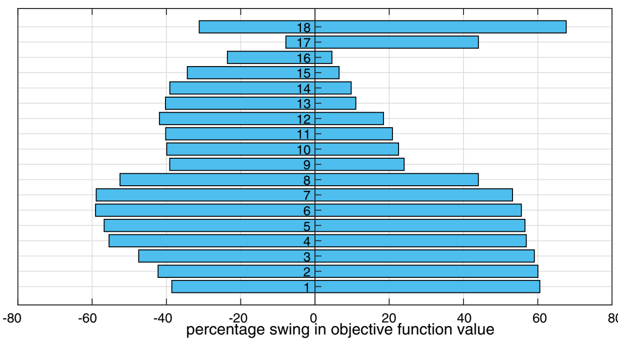

Fig. 4 Tornado diagram for sensitivity analysis with $\theta_i = 1 \pm 0.1; i = 1, \ldots, 18$

moment-free pin connection as per design. Thus, the additional moments affect the modal frequencies while the truss members (which are no longer co-planar) are less effective in force transfer. Hence, the bridge shows more deflection under static load. The member stiffness values need to be updated to replicate this behaviour in the finite element model so that the identified modal frequencies match with the model predicted frequencies. For this purpose, the joint stiffness is factored by an unknown parameter (θ), which is updated using the proposed HMC-based Bayesian inference. Since the members experience partial fixity at the ends due to distortion, they are modelled as beam elements instead of bar elements as in the initial model. Young's modulus (E) of the affected members are multiplied by the factor θ_i to update their stiffness. As the stiffness of a beam element is expressed in terms of ($\frac{EI}{L^3}$), updating Young's modulus leads to the proportionate change in member stiffness.

The structure has 40 joints (i.e. 18 top and 22 bottom), among which the joints on the right half of the bridge are affected most (as marked in Fig. 1b). Thus, a sensitivity analysis is performed using a tornado chart to identify the most critical joints. In this analysis, the change of the objective function corresponding to a 10% change (i.e. increase or decrease) of the stiffness is studied. The percentage change of the objective function value corresponding to 10% change in the joint stiffness is plotted on the either side of the vertical axis in Fig. 1. The joint locations leading to maximum change in the objective function value are then selected as the most sensitive joints. This analysis is performed using 18 top joints as the bottom joints are found to be insensitive due to the presence of the thick deck slab at that level. The tornado chart in Fig. 4 reveals that joints 1–14 and 18 have a significant impact on the objective function. However, the survey data presented in Fig. 1 reveal that only four joints in the right half (i.e. 4, 5, 6, and 7 which fall over the grid line 9–9 and 10–10 in Fig. 1) have suffered maximum misalignment. Thus, two different cases are considered in this study to cover all possible options. In the first case, 15 joints identified from the tornado diagram (i.e. Case I) are used to update the model. In the second option, 4 joints identified from the site survey are used, which are also identified in the tornado chart (i.e. Case II). In this context, the rolling vibration (observed during the field experiment and the wavelet analysis of horizontal response) suggests that the 4 joints in Case II are critical, which are envisaged to excite the torsional mode of vibration (i.e. second mode as shown in Fig. 10b).

As stated earlier, affected joints are factored by θ_i to modify the stiffness of the associated members. These parameters are then modified through the proposed iterative model updating algorithm, ultimately resulting in joint stiffness calibration. Since the natural frequency of the structure is used as a performance measure to quantify the agreement between the as-built bridge and FE model, the likelihood function is formed using the following expressions

$$p(D|\theta, C) = K_0 \exp\left[-\frac{J_g(\theta)}{2\epsilon_i^2}\right] \tag{14a}$$

$$J_g(\theta) = \frac{1}{N}\sum_{n=1}^{N}\left[\frac{f_{n_{\mathrm{act}}}^2 - f_{n_{\mathrm{mod}}}(\theta)^2}{f_{n_{\mathrm{act}}}^2}\right]^2 \tag{14b}$$

Here, $f_{n_{\mathrm{act}}}$ represents the identified or actual in-situ modal frequency and $f_{n_{\mathrm{mod}}}(\theta)$ is the model predicted frequency for a particular value of θ_i. The first three fundamental frequencies are used in Eq. (14a) to update the FE model in this study. It may be noted that only identified natural frequencies are used to develop the objective function instead of the general practice that also involves mode shapes or modal strain energies due to the low-density instrumentation used in this study, which is not reliable for mode shape estimation. A weighted objective function is constructed using the in-situ modal frequencies, where the weights are decided based on the mass participation factors. Thus, 60% weight is assigned to the first natural frequency, while 30% and 10% weights are assigned to the second and third natural frequencies, respectively. The prior pdf for this algorithm is assumed to follow independent Gaussian distribution centered at the original value of $\theta_i = 1; i = 1, \ldots, 4$. The COV is assumed to be unity to avoid any bias in accepting or rejecting a candidate, and an adaptive scheme is constructed using $r = \frac{1}{\sqrt{3}}$ and $k = 1$. A detailed discussion on selecting relevant parameters of this bridge is provided by Baisthakur and Chakraborty [37].

Table 2 Comparison of identified and updated modal frequencies in Test 1

Mode number	$f_{n_{in}}$ (Hz)	$f_{n_{id}}$ (Hz)	$f_{n_{upd}}$ (Hz)	
			Case I	Case II
1	2.396	2.733 [14.06]	2.569 [05.98]	2.612 [04.43]
2	4.349	4.122 [05.22]	4.319 [04.79]	4.293 [04.15]
3	4.940	5.061 [02.45]	5.061 [00.01]	5.033 [00.55]

Values within parenthesis represent % error

7 Numerical results and discussions

This section presents the results obtained from the experimental verification of the proposed Hamiltonian Monte Carlo-based finite element model updating, followed by the load rating. First, the performance of the proposed improved Bayesian inference for digital model calibration is discussed. The updated model is finally used for the capacity estimation, i.e. rating.

7.1 Diagnostic test for load rating of Truss bridge

The model is updated to match the identified modal frequencies obtained from the wavelet-based clustering of the acceleration responses. The first three identified frequencies are shown in Table 2 where f_n represents the modal frequencies in Hz. The secondary subscripts in, id and upd in this table correspond to the initial, identified and updated values, respectively. Two different model classes are used where Case I and Case II have 15 and 4 unknown parameters (i.e. θ_i). The comparisons of natural frequencies before and after the model updating are also presented in the same table, where the results from Test 1 are shown for brevity. The nature of compliance between the observed values and

Table 3 Updated values of θ_i in Case I

Parameter	Initial value	Updated value	Std. deviation	Cov (%)
θ_1	1	2.5049	0.1305	05.24
θ_2	1	1.7434	0.0222	01.29
θ_3	1	0.4018	0.0343	07.47
θ_4	1	1.5978	0.0559	03.70
θ_5	1	2.8103	0.0980	03.71
θ_6	1	2.4251	0.1662	06.39
θ_7	1	1.2464	0.0853	07.13
θ_8	1	1.3463	0.0175	01.31
θ_9	1	2.2221	0.0588	02.51
θ_{10}	1	0.4468	0.0376	08.25
θ_{11}	1	0.6706	0.0074	01.11
θ_{12}	1	1.0473	0.0403	04.31
θ_{13}	1	2.3329	0.2196	12.22
θ_{14}	1	2.3594	0.0455	01.86
θ_{15}	1	2.9106	0.0334	01.17

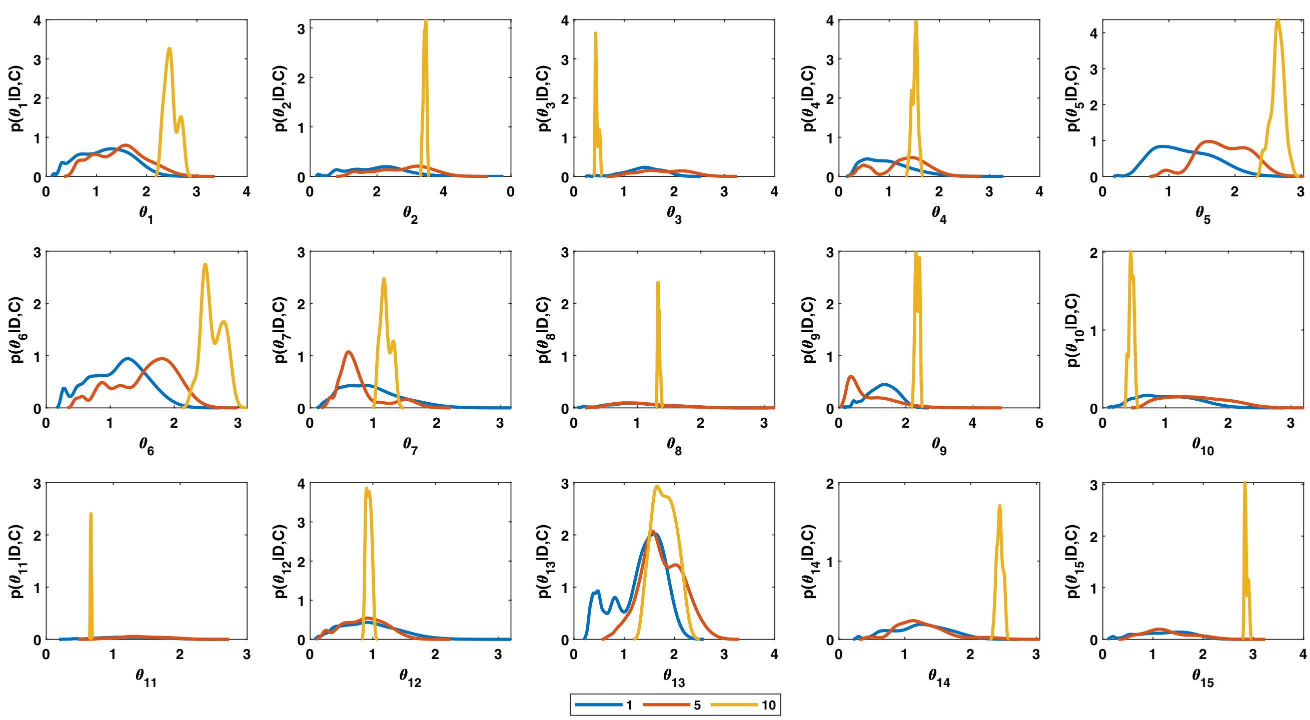

Fig. 5 Marginal posterior distribution of θ_i in Case I

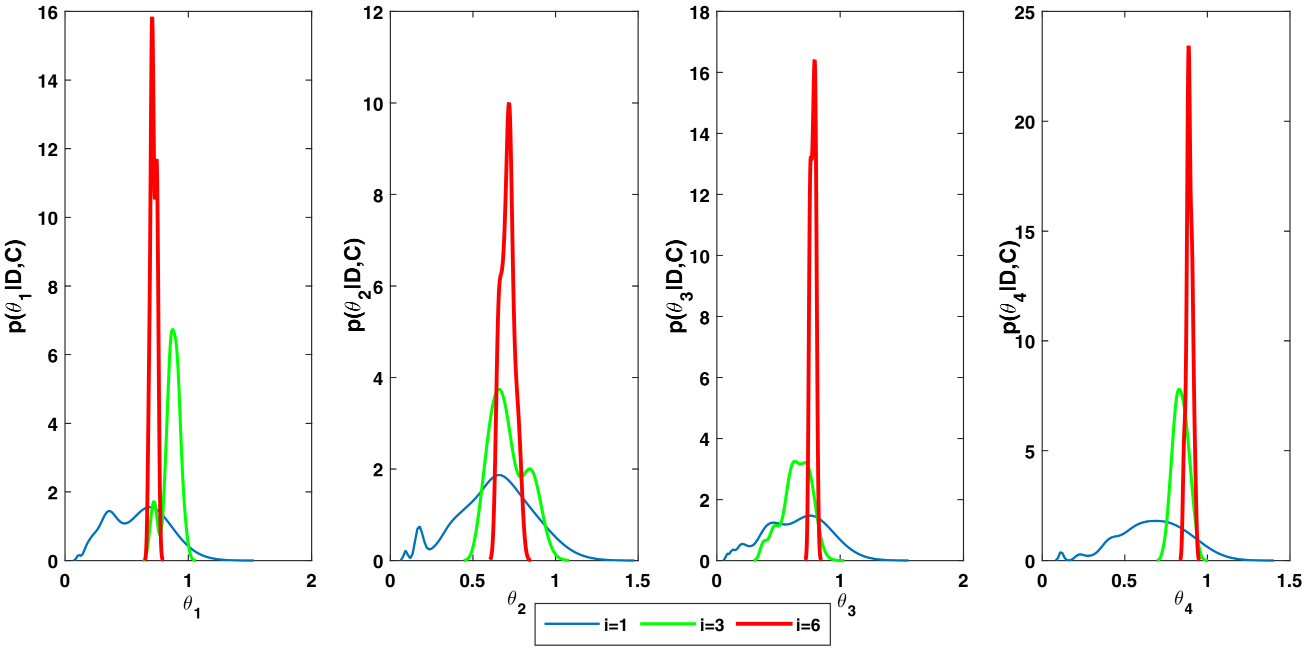

Fig. 6 Marginal posterior distribution of θ_i in Case II

the two different cases indicates that they replicate the in-situ modal behaviour with gross error within 10%. Therefore, these two models can be adopted for further analysis. In this updating process, an adaptive search is used where the posterior distribution of θ_i gradually converges to its final form as the iteration progresses. The posterior pdf sequence obtained from two different cases conditioned by measurement **D** and model class **C** is shown in Figs. 5 and 6. Case I converges in ten iterations, while Case II needs six iterations before the error falls below the allowable limit of 1%. Fig. 5 shows posterior pdfs for 1st, 5th and 10th iterations for Case I. The updated values of the uncertain parameters in Case I are presented in Table 3,

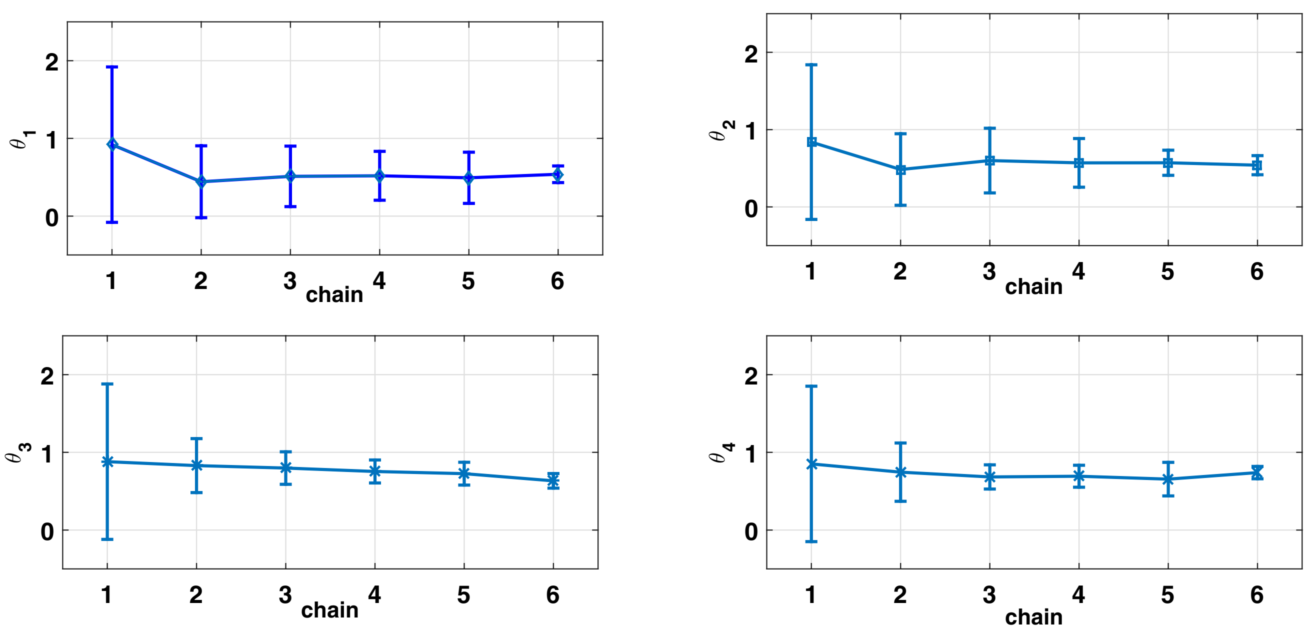

Fig. 7 Standard deviation of *theta*$_i$ in different iteration for Case II

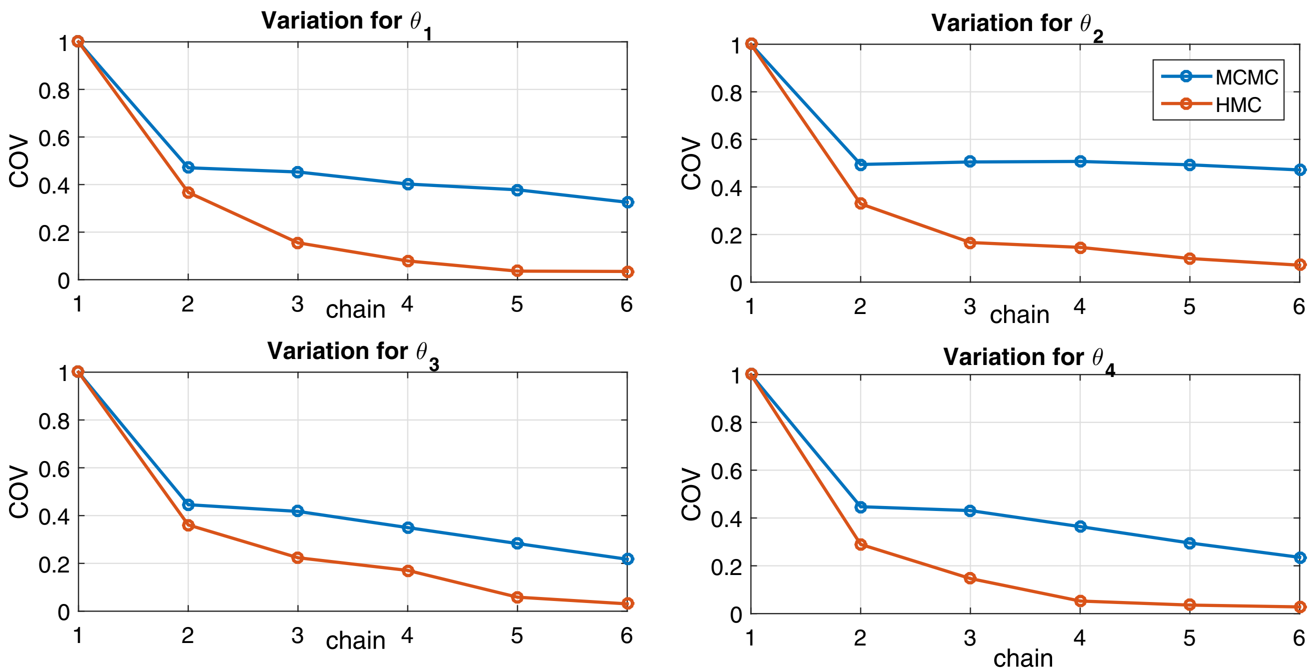

Fig. 8 Rate of convergence of the proposed HMC and the conventional MCMC algorithm in Case II

which indicate a significant change in the member stiffness. Although these changes in stiffness offer excellent match with the modal behaviour, a close review of the values in Table 3 reveals unrealistic changes obtained in this case. In some members, the stiffness is increased by more than 2.5 times its original value. These unrealistic changes in some members correspond to those joints that have little or insignificant impact of misalignment (refer to Fig. 1b for joints on the left half of the bridge). These joints are selected from the tornado diagram, many of them do not comply with the field condition. Further analysis is carried out using Case II, where the joints are selected based on the sensitivity analysis and actual site survey. Figure 6 shows the posterior pdf of the updated parameters θ_i in the 1st, 3rd and 6th iterations. The converged values of the unknown parameters are also reported in Table 4. These updated parameter values indicate that the members connected to the four joints updated in Case II suffer a significant reduction of their member stiffness due to misalignment, which is consistent with the in-situ condition. Moreover, the modal frequencies also closely match with the identified values, as shown in Table 2. Therefore, the updated model in Case II is more realistic to replicate the bridge with misaligned joints, which is used for further analysis.

The unknown parameters θ_i gradually converge to their most probable values and the mean and standard deviation of these parameters in Case II for different chains are shown in Fig 7. This figure demonstrates the reduction of co-variance of θ_i as the iteration progresses.

These results in Table 4 reveal that the four selected truss joints, which was initially designed as pinned connection, experience significant partial fixity. The updated

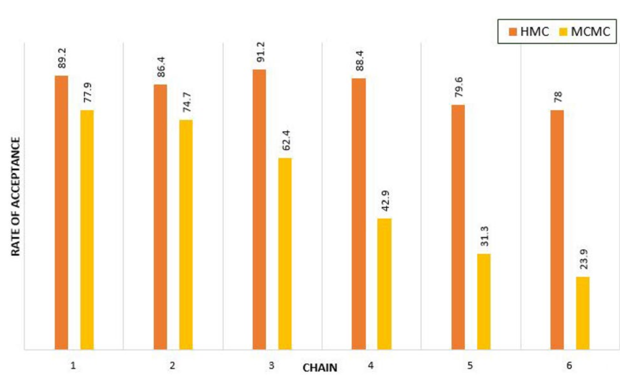

Fig. 9 Rate of acceptance of the proposed HMC and the conventional MCMC algorithm in Case II

Table 4 Updated values of θ_i in Case II

Parameter	Initial value	Updated value	Std. deviation	Cov (%)
θ_1	1	0.5385	0.0690	10.70
θ_2	1	0.5400	0.0706	12.35
θ_3	1	0.6333	0.0682	09.39
θ_4	1	0.7394	0.0528	07.95

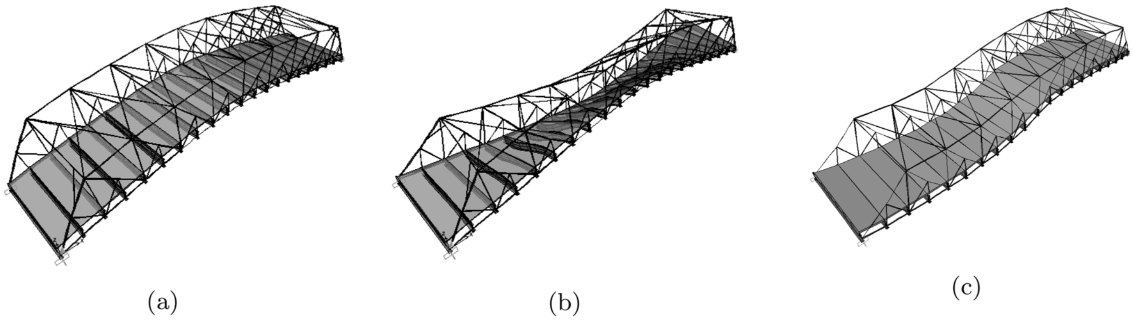

Fig. 10 Updated mode shapes of the bridge; **a** 1st mode, **b** 2nd mode and **c** 3rd mode

joints provide the stiffness of the order of 53.85%, 54.00%, 63.33%, and 73.94% as that of the fully fixed joints, and the uncertain parameters are consistent with the actual joint conditions. Since these joints (designed for transmitting axial loads only in the vertical plane) are subjected to end moments, it has induced unanticipated moments in the connected members. The rating-factor analysis is carried out using the updated finite element model to study the impact of misalignment on the load-carrying capacity of the bridge.

Once the model is updated by the proposed HMC-based Bayesian inference, its performance is compared with the Markov Chain Monte Carlo (MCMC) simulation using the Modified Metropolis–Hastings (MMH) algorithm for candidate generation. The MCMC approach needs more iterations for convergence, which leads to more number of model evaluations. The convergence rate offered by the proposed HMC algorithm and the conventional MCMC algorithm is demonstrated in Fig. 8 for the same number of iterations. From this figure, it is clear that the proposed HMC approach can efficiently explore the parameter space and rapidly converge to the high probability region of θ_i with less number of iterations and hence, demands less computational cost. Also, the adaptive scheme presented in this study (i.e. Eqs. 13a and b) is found to be more efficient than the conventional MCMC-based approach as it maintains a consistent rate of acceptance of the candidate states across all chains. In contrast, the acceptance rate in conventional MCMC decreases with the increase in the number of chains presented in Fig. 9. The closed-form solution for candidate generation proposed in this study offers more acceptance at a aster rate compared to the random walk-based MMH algorithm. It is reflected in every iteration, as demonstrated in Fig. 9.

7.1.1 Rating factor analysis

In this section, the effect of joint distortion on the load rating is presented using the finite element model obtained from Bayesian updating. The updated model in Case II is used to conduct a virtual proof load test by exposing the

Fig. 11 Vehicular load models

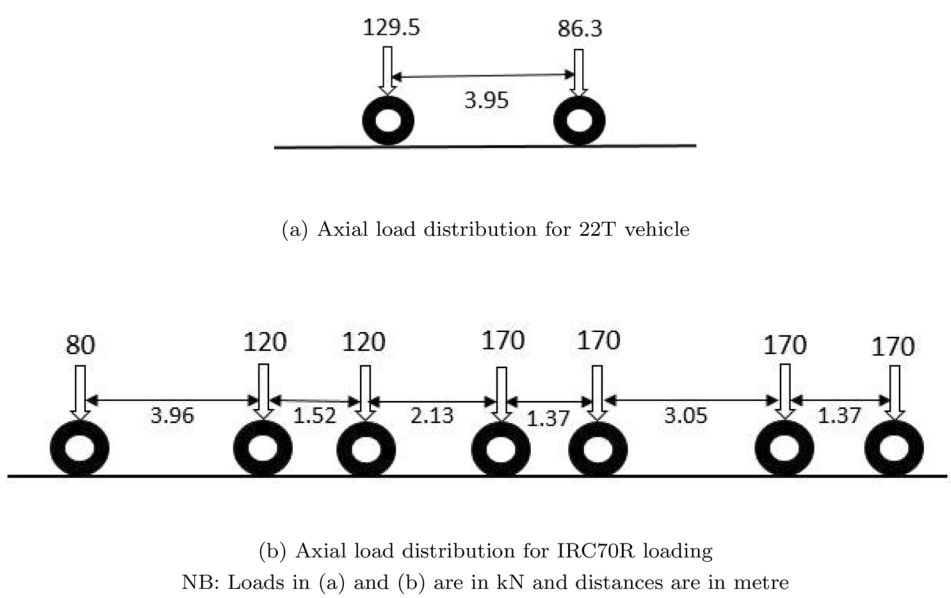

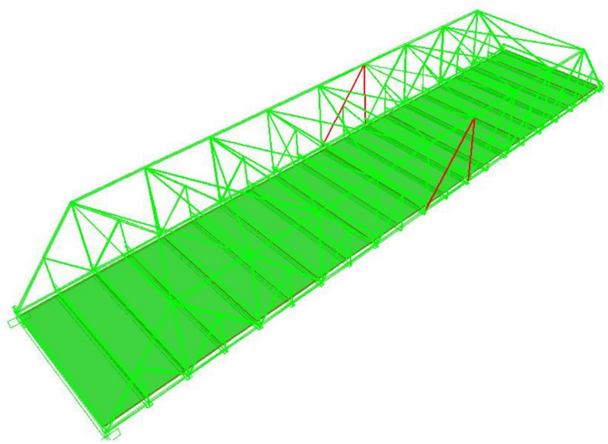

Fig. 12 Members with rating factor less than one for operating condition

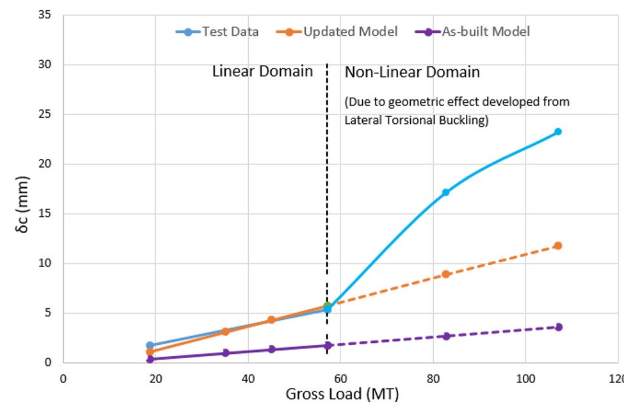

Fig. 13 Deflection pattern observed at site and in as-built and updated finite element model

bridge model to different classes of live loads in SAP2000. The first three modes of the bridge obtained from the updated model are shown in Fig. 10. The second mode, in particular, is responsible for the torsional vibration, which is excited due to misalignment, as noticed in the scalogram (refer to Fig. 3d) and during the experiment. Since the updated model replicates the as-built bridge behaviour, this model predicted response for the proof load is expected to forecast the response realistically. The forces generated in different members in this virtual live load analysis are recorded for their subsequent use in rating analysis, where vehicles of different load classes traverse along the centre line of the bridge.

In this process, the vehicle is allowed to pass over the bridge at a constant velocity of 20 kmph and the forces generated in the members are recorded, which are used to compute the rating factor using Eq. (3). In this study, the load rating is performed at two levels (i.e. inventory and operating condition). For the inventory rating, the 22T vehicle used in the diagnostic test passes over the bridge at 20 kmph. The equivalent point load model of this vehicle is shown in Fig. 11a and the parameters γ_{DL} and γ_{LL} are assumed to be 1.5 and 1.35 [58], respectively. The rating factors obtained from this analysis are reported in Table 5, where the minimum factor is 2.34. It indicates the availability of sufficient member strength for this load class.

For the operating load rating, IRC70R wheeled vehicle is used as this is the designed load class. The point load model of this vehicle is presented in Fig. 11b, which has a total weight of 1000 kN. The factors γ_{DL} and γ_{LL}, in this case, are assumed to be 1.5, and 1.75 [58], respectively, along with the appropriate impact factor as per the IRC:6 [49] guidelines. The rating factors for this case show that four members have values less than 1 (refer to Table 5, which are highlighted in Fig 12. Here, it may be noted that the bridge experiences severe rolling as the torsional mode is excited during the experiment. Since the joints on the right half of the bridge are mostly affected by the misalignment and subsequent strength degradation, the members on the right half experience redistribution of forces (beyond its designed values), ultimately affecting their load-carrying capacity and the rating factor.

Finally, the load-deflection behaviour of the bridge is investigated and compared with the static load test data, as shown in Fig. 13. The vertical line in this figure demarcates two distinct regions where the linearity is dominant on the left-hand side. As the load intensity increases, the lateral-torsional deflection of the bridge sets in, affecting the geometric stiffness leading to unwanted deformation not envisaged in the design. However, the linear behaviour shifts from its initial model to the updated model and matches

Table 5 Inventory rating factor comparison of the initial and updated model using test data

Sr no.	Section name	As per design		Test-1		Test-2		Test-3	
		Op	Inv	Op	Inv	Op	Inv	Op	Inv
1	Sec15-L6	5.32	1.47	2.34	0.45	2.47	0.48	2.60	0.51
2	Sec15-R6	5.32	1.47	2.60	0.50	2.52	0.49	2.93	0.57
3	Sec11-R6	7.62	1.94	4.75	0.93	4.76	0.96	4.77	0.97
4	Sec11-L6	7.62	1.94	4.82	0.97	4.90	0.97	4.81	1.06

Op and Inv represent operating and inventory levels, respectively closely with the test data, which in turn ensures the accuracy of the proposed updating methodology. This behaviour is projected further (i.e. dotted lines) to demonstrate the difference between the modelled behaviour and in-situ condition originating from the misalignment of truss joints. The process (i.e. rating factor evaluation) is repeated for Test-2 and Test-3, and the results are reported in Table 5. These factors are compared with their designed value to study the impact of joint distortion. It indicates a minor misalignment of joints (i.e. < 0.5% of span) can reduce the rating factor by more than 100%. This reduction of rating factor below 1 highlights a potential weak link in the truss, which can act as the initial point of a catastrophic failure. Since the inventory level analysis indicates adequate member strength, it is referred to as the load-carrying capacity of the bridge i.e. 22T.

8 Conclusion

The present work investigates the load rating of a steel truss bridge using modified Hamiltonian Monte Carlo-based model updating. The proposed approach has a considerable advantage over conventional Markov Chain Monte Carlo simulation using modified Metropolis–Hastings algorithm in terms of the computational cost. The numerical results show the efficiency of the proposed method to replicate the field behaviour accurately. The steel bridge used in this study is a unique example of misaligned truss joints that experience partial fixity. The experimental results demonstrate the impacts of joint misalignment in terms of the modal frequencies and load-carrying capacity of the bridge. In this context, the proposed HMC algorithm uses the commercial finite element package to develop the digital twin of the actual bridge to carry out proof load test numerically for rating analysis. Hence, the proposed algorithm works as a viable alternative to the actual proof load test, which involves the potential risk of permanently damaging the bridge. Besides these observations, the major lessons learned from this study are

1. Full-scale bridge load testing is a challenging task, especially for those structures at remote locations and in rugged terrain. These issues often lead to low-density instrumentation using only wireless sensors, which are easy to install and operate. Under these scenarios, time-frequency based signal processing is a dependable alternative to track the in-situ dominant modes.
2. These identified modes help to update the finite element model that works as a digital twin of the original bridge and avoid the physical proof load test for its rating. Due to this reason, the safety of the bridge is never compromised. Hence, the overall cost involved in the rating analysis is much less as it does not invoke any additional precautionary measures.
3. The model calibration using optimization in the Bayesian framework performs better when the initial model is realistic and close to the in-situ conditions. It is demonstrated using two different models where Case I uses the tornado diagram to select the joints for updating. It works as a black-box and does not combine other information available from the actual survey of the in-situ conditions. While Case II utilizes both sensitivity analysis and other valuable information, i.e., misaligned joints. In both cases, the updated modal frequencies match the identified values well, indicating the convergence of the iterative process. The numerical optimization can adjust the stiffness and other parameters of different members to match the eigen values, which may not be unique always. However, the rating analysis shows that the second model offers meaningful results, closely matching the field condition.
4. The HMC-based Bayesian model updating converges faster as the closed-form candidate generation scheme is computationally efficient. It is beneficial for large/complex finite element models due to its higher acceptance rate and faster convergence.

Overall, the experimental investigation presented in this work shows the performance of the proposed HMC-based model updating for capacity estimation of a bridge in light of the practical challenges. The numerical studies show the potential of the detailed digital simulation in the Bayesian framework and its efficiency for load rating of existing bridges. It also indicates the scope for further improvements by incorporating other critical phenomena, such as loaded-length effect, floating axle loads, and braking/acceleration effects. These issues need more analytical and experimental investigations, which open up the avenues of further research on this topic.

Appendix

The geometric details and member names are shown in Figs. 14 and 15. The structural steel sections are given in Table 6 while the member properties used to model this bridge are provided in Table 7.

Table 6 Frame section details of Pasakha Bridge

Frame label	Section	Frame label	Section	Frame label	Section
22	Sec3-R1	82	Sec1-R6	151	Sec2-L7
23	Sec3-R1	83	Sec17	152	Sec1-L4
24	Sec3-R2	84	Sec17	153	Sec1-L4
25	Sec3-R2	85	Sec17	154	Sec1-L5
26	Sec3-R10	86	Sec17	155	Sec1-L6
27	Sec3-R10	87	Sec17	156	Sec12-L1
28	Sec3-R9	88	Sec17	157	Sec12-L9
29	Sec3-R9	89	Sec17	158	Sec13-L2
30	Sec3-L1	90	Sec17	159	Sec13-L8
31	Sec3-L1	91	Sec17	160	Sec14-L3
32	Sec3-L2	92	Sec17	161	Sec14-L7
33	Sec3-L2	93	Sec18	162	Sec15-L4
34	Sec3-L10	94	Sec18	163	Sec15-L6
35	Sec3-L10	96	Sec18	164	Sec16-L5
36	Sec3-L9	98	Sec18	165	Sec8-L2
37	Sec3-L9	100	Sec18	166	Sec8-L2
38	Sec4-R3	105	Sec18-R6	167	Sec8-L9
39	Sec4-R3	107	Sec18-R7	168	Sec8-L9
40	Sec4-R8	109	Sec18-R10	169	Sec9-L3
41	Sec4-R8	110	Sec18-R10	170	Sec9-L3
42	Sec4-L3	111	Sec12-R1	171	Sec9-L8
43	Sec4-L3	112	Sec12-R9	172	Sec9-L8
44	Sec4-L8	113	Sec13-R2	173	Sec10-L4
45	Sec4-L8	114	Sec13-R8	174	Sec10-L4
54	Sec5-R4	115	Sec14-R3	175	Sec10-L7
55	Sec5-R4	116	Sec14-R7	176	Sec10-L7
56	Sec5-R7	117	Sec15-R4	177	Sec11-L5
57	Sec5-R7	118	Sec15-R6	178	Sec11-L5
58	Sec5-L4	119	Sec16-R5	179	Sec11-L6
59	Sec5-L4	128	Sec8-R2	180	Sec11-L6
60	Sec5-L7	129	Sec8-R2	181	Sec17
61	Sec5-L7	130	Sec8-R9	182	Sec17
62	Sec6-R5	131	Sec8-R9	183	Sec17
63	Sec6-R5	132	Sec9-R3	184	Sec17
64	Sec6-R6	133	Sec9-R3	185	Sec17
65	Sec6-R6	134	Sec9-R8	186	Sec17
67	Sec6-L5	135	Sec9-R8	187	Sec17
68	Sec6-L5	136	Sec10-R4	188	Sec17
69	Sec6-L6	137	Sec10-R4	189	Sec17
70	Sec6-L6	138	Sec10-R7	190	Sec17
71	Sec7-R1	139	Sec10-R7	191	Sec18
72	Sec7-R1	140	Sec11-R5	192	Sec18
73	Sec7-R10	141	Sec11-R5	193	Sec18
74	Sec7-R10	142	Sec11-R6	194	Sec18
75	Sec2-R1	143	Sec11-R6	195	Sec18
76	Sec2-R2	144	Sec7-L1	196	Sec18-L5
77	Sec2-R8	145	Sec7-L1	197	Sec18-L6
78	Sec2-R7	146	Sec7-L10	198	Sec18-L7
79	Sec1-R3	147	Sec7-L10	199	Sec18-L10

Table 6 (continued)

Frame label	Section	Frame label	Section	Frame label	Section
80	Sec1-R4	148	Sec2-L1	200	Sec18-L10
81	Sec1-R5	149	Sec2-L2		
82	Sec1-R6	150	Sec2-L8		

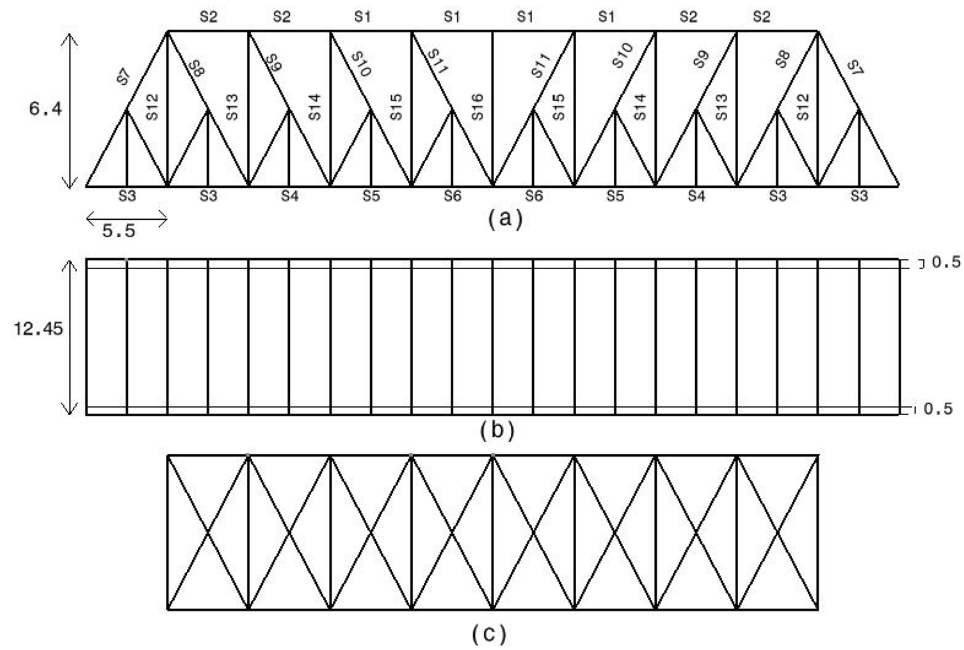

Fig. 14 Dimensions of Pasakha bridge; **a** elevation @ $Y =$ 0/12.45 m **b** plan view @ Z = 0 m **c** plan view @ $Z = 6.4$ m i All the short vertical and inclined members in subfig (a) are S17 and S18, respectively ii All the transverse girders in subfig (b) are Cross-beam (DB) iii All the transverse bracing in subfig (c) are B1 and cross beams are BXB1

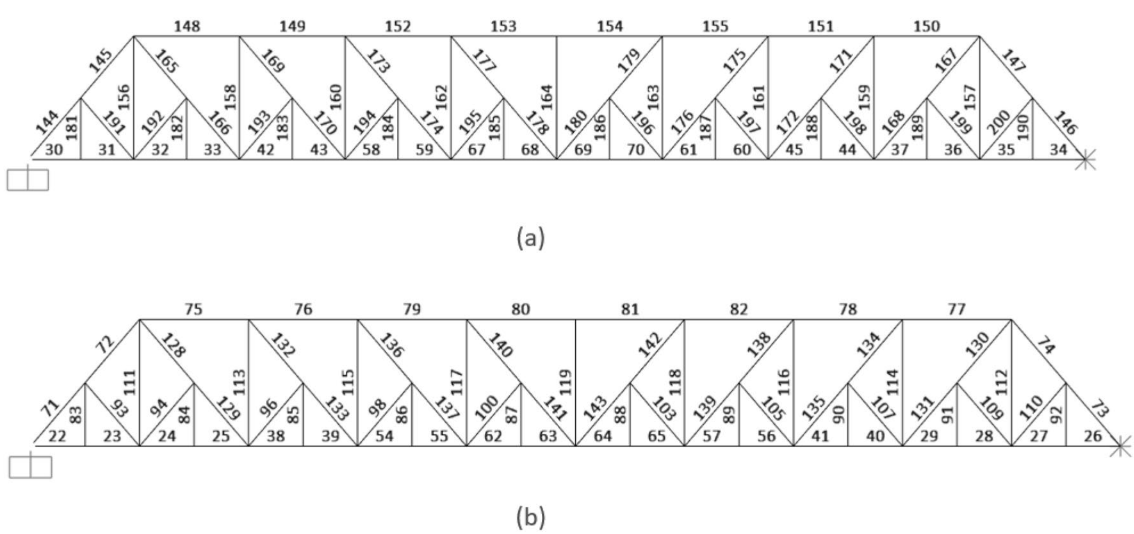

Fig. 15 Elevation of Pasakha Bridge; **a** left truss and **b** right truss

Table 7 Member details i.e. cross-section of Pasakha bridge

Section name	Area (m^2)	Section name	Area (m^2)
B1	0.0068	B2	0.0091
BXB1	0.005	DB	0.0188
S1	0.047	S2	0.037
S3	0.0292	S4	0.0314
S5	0.0394	S6	0.0437
S7	0.041	S8	0.021
S9	0.0198	S10	0.012
S11	0.0068	S12	0.009
S13	0.0154	S14	0.0125
S15	0.0045	S16	0.0045
S17	0.0038	S18	0.0086

Acknowledgements This publication resulted from the research supported by the DST, Govt. of India, Science and Engineering Research Board Grant No. CRG/2020/005090.

Declarations

Conflict of interest The authors declare that they have no known competing financial interests or personal relationships that could have appeared to influence the work reported in this paper.

References

1. Subcommittee on Bridges TOS (2000) Manual for condition evaluation of bridges, 1994. American Association of State Highway and Transportation Officials, Washington
2. Phares BM, Washer GA, Rolander DD, Graybeal BA, Moore M (2004) Routine highway bridge inspection condition documentation accuracy and reliability. J Bridge Eng 9(4):403–413
3. Breña SF, Jeffrey AE, Civjan SA (2013) Evaluation of a noncomposite steel girder bridge through live-load field testing. J Bridge Eng 18(7):690–699
4. Moses F, Lebet JP, Bez R (1994) Applications of field testing to bridge evaluation. J Struct Eng 120(6):1745–1762
5. Saraf V, Nowak AS (1998) Proof load testing of deteriorated steel girder bridges. J Bridge Eng 3(2):82–89
6. Casas JR, Gómez JD (2013) Load rating of highway bridges by proof-loading. KSCE J Civ Eng 17(3):556–567
7. Boothby TE, Craig RJ (1997) Experimental load rating study of a historic truss bridge. J Bridge Eng 2(1):18–26
8. Cheung MS, Tadros G, Brown T, Dilger W et al (1997) Field monitoring and research on performance of the confederation bridge. Can J Civ Eng 24(6):951
9. Bakht B (1981) Testing of the manitou bridge to determine its safe load carrying capacity. Can J Civ Eng 8(2):218–229
10. Lantsoght E, van der Veen C, de Boer A, Hordijk DA (2017) Proof load testing of reinforced concrete slab bridges in the Netherlands. Struct Concr 18(4):597–606
11. Stewart MG, Val DV (1999) Role of load history in reliability-based decision analysis of aging bridges. J Struct Eng 125(7):776–783
12. Faber MH, Val DV, Stewart MG (2000) Proof load testing for bridge assessment and upgrading. Eng Struct 22(12):1677–1689
13. Fu G, Tang J (1995) Risk-based proof-load requirements for bridge evaluation. J Struct Eng 121(3):542–556
14. Shah SP, Popovics JS, Subramaniam KV, Aldea C-M (2000) New directions in concrete health monitoring technology. J Eng Mech 126(7):754–760
15. Doebling SW, Farrar CR, Prime MB et al (1998) A summary review of vibration-based damage identification methods. Shock Vib Dig 30(2):91–105
16. Wong K-Y (2004) Instrumentation and health monitoring of cable-supported bridges. Struct Control Health Monit 11(2):91–124
17. Al-Khateeb HT, Shenton HW, Chajes MJ (2018) Computing continuous load rating factors for bridges using structural health monitoring data. J Civ Struct Health Monit 8(5):721–735
18. Bakht B, Jaeger LG (1990) Bridge testing—a surprise every time. J Struct Eng 116(5):1370–1383
19. Bakht B, Jaeger LG (1988) Bearing restraint in slab-on-girder bridges. J Struct Eng 114(12):2724–2740
20. Bakht B, Jaeger LG (1992) Ultimate load test of slab-on-girder bridge. J Struct Eng 118(6):1608–1624
21. Chajes MJ, Mertz DR, Commander B (1997) Experimental load rating of a posted bridge. J Bridge Eng 2(1):1–10
22. Jáuregui DV (1999) Measurement-based evaluation of non-composite. PhD Thesis, University of Texas, Austin, USA
23. Wang N, O'Malley C, Ellingwood BR, Zureick A-H (2011) Bridge rating using system reliability assessment. I: Assessment and verification by load testing. J Bridge Eng 16(6):854–862
24. Catbas FN, Gokce HB, Gul M (2012) Practical approach for estimating distribution factor for load rating: demonstration on reinforced concrete t-beam bridges. J Bridge Eng 17(4):652–661
25. Dong C, Bas S, Debees M, Alver N, Catbas FN (2020) Bridge load testing for identifying live load distribution, load rating, serviceability and dynamic response. Front Built Environ 6:46
26. Lrfd A (2017) Aashto lrfd bridge design specifications. American Association of State Highway and Transportation Officials, Washington
27. Yost JR, Schulz JL, Commander BC (2005) Using NDT data for finite element model calibration and load rating of bridges. In: Structures Congress 2005: Metropolis and Beyond, pp 1–9
28. Turer A, Shahrooz BM (2011) Load rating of concrete-deck-on-steel-stringer bridges using field-calibrated 2d-grid models. Eng Struct 33(4):1267–1276
29. Sanayei M, Phelps JE, Sipple JD, Bell ES, Brenner BR (2012) Instrumentation, nondestructive testing, and finite-element model updating for bridge evaluation using strain measurements. J Bridge Eng 17(1):130–138
30. Beck JL, Katafygiotis LS (1998) Updating models and their uncertainties. I: Bayesian statistical framework. J Eng Mech 124(4):455–461
31. Katafygiotis LS, Papadimitriou C, Lam H-F (1998) A probabilistic approach to structural model updating. Soil Dyn Earthq Eng 17(7–8):495–507
32. Beck JL, Au S-K (2002) Bayesian updating of structural models and reliability using Markov Chain Monte Carlo simulation. J Eng Mech 128(4):380–391
33. Ching J, Chen Y-C (2007) Transitional Markov Chain Monte Carlo method for bayesian model updating, model class selection, and model averaging. J Eng Mech 133(7):816–832
34. Cheung SH, Beck JL (2009) Bayesian model updating using hybrid Monte Carlo simulation with application to structural dynamic models with many uncertain parameters. J Eng Mech 135(4):243–255
35. Duane S, Kennedy AD, Pendleton BJ, Roweth D (1987) Hybrid Monte Carlo. Phys Lett B 195(2):216–222

36. Wang Z, Broccardo M, Song J (2019) Hamiltonian Monte Carlo methods for subset simulation in reliability analysis. Struct Saf 76:51–67
37. Baisthakur S, Chakraborty A (2020) Modified Hamiltonian Monte Carlo-based Bayesian finite element model updating of steel truss bridge. Struct Control Health Monit 27(8):e2556
38. Hasançebi O, Dumlupınar T (2013) Detailed load rating analyses of bridge populations using nonlinear finite element models and artificial neural networks. Comput Struct 128:48–63
39. Alipour M, Harris DK, Barnes LE, Ozbulut OE, Carroll J (2017) Load-capacity rating of bridge populations through machine learning: application of decision trees and random forests. J Bridge Eng 22(10):04017076
40. Seo J, Czaplewski TM, Kimn J-H, Hatfield G (2015) Integrated structural health monitoring system and multi-regression models for determining load ratings for complex steel bridges. Measurement 75:308–319
41. Kim YJ, Queiroz LB (2017) Big data for condition evaluation of constructed bridges. Eng Struct 141:217–227
42. Seo J, Phares B, Lu P, Wipf T, Dahlberg J (2013) Bridge rating protocol using ambient trucks through structural health monitoring system. Eng Struct 46:569–580
43. Akgül F, Frangopol DM (2004) Time-dependent interaction between load rating and reliability of deteriorating bridges. Eng Struct 26(12):1751–1765
44. Akgül F, Frangopol DM (2004) Bridge rating and reliability correlation: comprehensive study for different bridge types. J Struct Eng 130(7):1063–1074
45. Wang N, Ellingwood BR, Zureick A-H (2011) Bridge rating using system reliability assessment. II: improvements to bridge rating practices. J Bridge Eng 16(6):863–871
46. Alampalli S, Frangopol DM, Grimson J, Halling MW, Kosnik DE, Lantsoght EO, Yang D, Zhou YE (2021) Bridge load testing: state-of-the-practice. J Bridge Eng 26(3):03120002
47. Alampalli S, Frangopol DM, Grimson J, Kosnik D, Halling M, Lantsoght EO, Weidner JS, Yang DY, Zhou YE (2019) Primer on bridge load testing. Transportation Research Circular, Technical Report No. E-C257, Transportation Research Board, Washington DC, USA
48. IRC:SP:37-2010 (2010) Guidelines for evaluation of load carrying capacity of bridges. The Indian Road Congress, New Delhi
49. IRC:6-2017 (2017) Standard specifications and code of practice for road bridges, section-II loads and load combinations (seventh revision). The Indian Road Congress, New Delhi
50. IRC:24-2010 (2010) Standard specifications and code of practice for road bridges, section-V steel road bridges. The Indian Road Congress, New Delhi
51. IRC:78-2014 (2014) Standard Specifications and code of practice for road bridges, section VII–foundations and substructure, revised. The Indian Road Congress, New Delhi
52. IS:456-2000 (2000) Plain and reinforced concrete-code of practice. Bureau of Indian Standards, New Delhi
53. IRC:SP:51-1999 (1999) Guidelines for load testing of bridges. The Indian Road Congress, New Delhi
54. Mahato S, Chakraborty A (2019) Sequential clustering of synchrosqueezed wavelet transform coefficients for efficient modal identification. J Civ Struct Health Monit 9(2):271–291
55. Biggs JM, Suer HS (1956) Vibration measurements on simple-span bridges. Highway Research Board Bulletin, Technical Report No. 124, Massachusetts Institute of Technology, Cambridge, USA
56. Wright DT, Green R (1964) Highway bridge vibrations: part II, Ontario Test Programme. Queen's University, Belfast
57. Cantieni R (1983) Dynamic load tests on highway bridges in Switzerland, 60 years of experience of empa, report n. 211. EMPA
58. Sanayei M, Reiff AJ, Brenner BR, Imbaro GR (2016) Load rating of a fully instrumented bridge: comparison of lrfr approaches. J Perform Constr Facil 30(2):04015019